



A variable amplitude fretting fatigue life estimation technique: Formulation and experimental validation

C.T. Kouanga^a, J.D. Jones^b, I. Reville^c, A. Wormald^c, D. Nowell^d, R.S. Dwyer-Joyce^e,
L. Susmel^{a,*}

^a Department of Civil and Structural Engineering, the University of Sheffield, Sheffield S1 3JD, UK

^b Cummins Inc., Box 3005M/C 50020, Columbus, IN 47202-3005, USA

^c Cummins Daventry Technical Centre, Royal Oak Way South, Daventry NN11 8NU, UK

^d Department of Mechanical Engineering, Imperial College London, Kensington, London SW7 2AZ, UK

^e Department of Mechanical Engineering, the University of Sheffield, Sheffield S1 3JD, UK

ARTICLE INFO

Keywords:

Fretting fatigue
Variable amplitude
Fatigue life estimation
Critical distance
Multiaxial fatigue

ABSTRACT

The aims of the research work summarised in this paper are twofold. The first goal is to make available a large number of new experimental results generated by testing specimens of grey cast iron under both constant and variable amplitude fretting fatigue loading. The second goal is to formulate an advanced fretting fatigue design approach based on the combined use of the Modified Wöhler Curve Method, the Theory of Critical Distances and the Shear Stress-Maximum Variance Method. The validation exercise based on the experimental results being produced demonstrates that the proposed methodology is a powerful tool suitable for designing mechanical assemblies against fretting fatigue.

1. Introduction

Fretting fatigue is a damaging process that occurs at the interface between two contacting materials when they are subjected to cyclic tangential movements of small amplitude. As reported by Hills and Nowell [1], compared to the un-fretted condition, the presence of fretting can reduce the high-cycle fatigue strength of metallic materials by up to 50 %. This explains the reason why fretting fatigue is frequently a matter of concern in many important industrial sectors such as aeronautics and automotive. Accordingly, since the middle of the last century [2] to date much theoretical and experimental work has been done in order to develop accurate and reliable fretting fatigue life estimation techniques [3,4].

When it comes to designing metallic materials against fretting fatigue, the work done by Giannakopoulos et al. [5] arguably represents one of the most relevant breakthroughs in the field. In particular, by introducing the “notch analogue” concept, they postulated that the damaging processes taking place in notched metallic materials subjected to cyclic loading are the same as those observed under fretting fatigue. Based on this intuition, a number of follow-up studies attempted to extend to the fretting fatigue case the use of those methodologies that

were originally developed to deal with the standard notch fatigue problem [3,6].

As far as geometrical features of all kinds are concerned, examination of the state of the art suggests that the Theory of Critical Distances (TCD) [7,8] is one of the most successful approaches for modelling the detrimental effect of localised stress/strain concentration phenomena. The TCD quantifies fatigue damage via an effective design quantity that is calculated by adopting a material length scale parameter. This material length is used to directly post-process the stress/strain fields in the vicinity of the assessed notch [8]. Within this theoretical framework, the TCD critical distance is treated as a mechanical/fatigue property which is different for different materials and varies with load ratio [4].

While the TCD can be formulated in many different ways [10], the Point Method (PM) is not only the simplest form of this powerful theory, but also the most accurate and reliable one [7]. According to Peterson [11], the PM postulates that the stress state to be used to estimate fatigue damage has to be taken at a material-dependent distance from the apex of the notch.

Another important aspect characterising the fretting fatigue problem is that the stress/strain distributions in the contact regions are always multiaxial [1]. This explains the reason why, since the end of the 1980 s [12], several attempts have been made to extend to fretting fatigue the

* Correspondence to: Department of Civil and Structural Engineering, The University of Sheffield, Mappin Street, Sheffield S1 3JD, UK.

E-mail address: l.susmel@sheffield.ac.uk (L. Susmel).

<https://doi.org/10.1016/j.triboint.2022.108055>

Received 13 September 2022; Received in revised form 24 October 2022; Accepted 6 November 2022

Available online 9 November 2022

0301-679X/© 2022 The Authors. Published by Elsevier Ltd. This is an open access article under the CC BY license (<http://creativecommons.org/licenses/by/4.0/>).

Nomenclature	
A, B	Material fatigue constants in the L_M vs N_f relationship.
E	Young's modulus.
F(t)	Time-variable axial force applied to the fretting specimens.
F_a, F_m	Amplitude and mean value of force F(t).
$F_{a,i}$	Amplitude of the force associated with the i-th cycle.
$F_{a,max}$	Maximum amplitude of the force in the spectrum.
$F_{i,j,k}(t)$	External time-variable forces.
k	Negative inverse slope of the fully-reversed uniaxial fatigue curve.
k_0	Negative inverse slope of the fully-reversed torsional fatigue curve.
$k_{\tau}(\rho_{eff})$	Negative inverse slope of the modified Wöhler curve.
L_M	Critical distance in the finite life regime.
m	Mean stress sensitivity index.
$m_{\tau}(\rho_{eff})$	Negative inverse slope in the high-cycle fatigue regime under VA loading.
N_A	Reference number of cycles to failure.
N_b	Number of blocks to failure.
N_f	Experimental number of cycles to failure.
$N_{f,e}$	Estimated number of cycles to failure.
n_i	Number of cycles associated with the i-th force level in the spectrum.
N_{kp}	Number of cycles to failure defining the position of the knee point.
P(t)	Normal load pushing the pads against the fretting specimens.
P_a, P_m	Amplitude and mean value of force P(t).
P_S	Probability of survival.
r	Linear coordinate associated with the focus path.
R	Stress ratio ($R = \sigma_{min}/\sigma_{max}$ or $R = \tau_{min}/\tau_{max}$).
R_p	Pad radius.
t	Time instant.
$\Delta\sigma$	Range of the axial stress.
$\Delta\sigma_{A, 50\%}$	Range of the uniaxial endurance limit at N_A cycles to failure (for $P_S=50\%$).
$\Delta\sigma_{net}$	Range of the nominal net axial stress.
$\Delta\sigma_{An, 50\%}$	Range of the nominal net endurance limit at N_A cycles to failure (for $P_S=50\%$).
$\Delta\tau$	Range of the torsional stress.
$\Delta\tau_{A, 50\%}$	Range of the torsional endurance limit at N_A cycles to failure (for $P_S=50\%$).
ν	Poisson's ratio.
ρ_{eff}	Effective critical plane stress ratio.
ρ_{lim}	Intrinsic fatigue strength threshold.
σ_A	Amplitude of the fully-reversed uniaxial endurance limit at N_A cycles to failure.
σ_{An}	Amplitude of the fully-reversed uniaxial notch endurance limit.
$\sigma_b(t)$	Bulk stress at a generic instant.
σ_{max}, τ_{max}	Maximum stress in the cycle.
σ_{min}, τ_{min}	Minimum stress in the cycle.
$\sigma_{n,a}$	Amplitude of the stress perpendicular to the critical plane.
$\sigma_{n,m}$	Mean stress perpendicular to the critical plane.
$\sigma_{n,max}$	Maximum value of the stress perpendicular to the critical plane.
$\sigma_{n,min}$	Minimum value of the stress perpendicular to the critical plane.
σ_{UTS}	Ultimate tensile strength.
$\tau(t)$	Time-variable shear stress.
τ_a	Shear stress amplitude on the plane of maximum shear stress amplitude.
τ_A	Fully-reversed torsional endurance limit at N_A cycles to failure.
$\tau_{A, Ref}(\rho_{eff})$	Fatigue strength corresponding to N_{Ref} cycles to failure.
$\tau_{MV}(t)$	Resolved shear stress.
$\tau_{MV,max}$	Maximum value of the resolved shear stress.
$\tau_{MV,min}$	Minimum value of the resolved shear stress.

use of a variety of criteria originally developed to assess multiaxial fatigue damage [4] in plain metallic materials.

Given the historical perspective briefly summarised above, starting from the beginning of this century, a number of approaches have been formulated to attempt to assess fretting fatigue damage by combining the “notch analogue” concept – used in the form of the PM – with different multiaxial fatigue criteria - that include, amongst others: Dang Van's criterion [13,14], the Modified Wöhler Curve Method [15,16], Smith, Watson and Topper's parameter [17,18], Fatemi & Socie's method [18] and Findley's criterion [17]. In this setting, it is interesting to observe that, based on the outcomes from a bespoke experimental and theoretical investigation, Gandiolle et al. [19] came to the conclusion that, as far as fretting fatigue is concerned, the estimates obtained by using the critical plane concept are more accurate than those obtained from stress invariant-based criteria.

The considerations reported above are all based on studies involving the initiation of fretting fatigue cracks under constant amplitude (CA) cyclic loading. In this setting, the articles available in the technical literature show that, so far, the international scientific community has focused their attention mainly on CA fretting fatigue situations. In contrast, just a limited number of studies have been published to date [20–28] where the problem of quantifying and assessing fretting fatigue damage is addressed by considering variable amplitude (VA) load histories. As highlighted by Pinto et al. [29], the above studies are still limited and they cannot be used to draw any definitive conclusions, mainly because VA fretting fatigue failures were generated under coupled bulk and fretting load. Further, they observe that all the

post-processing analyses were based on uniaxial fatigue approaches so that the degree of multiaxiality of the stress/strain fields in the fretted regions was not taken into account explicitly. Finally, Pinto and co-authors [29] also highlight that still nothing can be concluded about the accuracy of a simple linear accumulation law (i.e., Palmgren and Miner's rule [30,31]) in assessing damage under VA fretting fatigue.

The considerations reported above make it evident that to date little work has been done in order to understand, model and assess damage in metallic materials subjected to VA fretting fatigue loading. In this challenging scenario, the ambitious aims of the research work summarised in what follows are twofold. The first goal is to make available to the international scientific community a large number of new experimental results generated under both CA and VA fretting fatigue loading by using a four-actuator cruciform fatigue machine. The second objective is to formulate a design approach based on the use of the Modified Wöhler Curve Method (MWCM) [32,33], the PM [7] and the Shear Stress-Maximum Variance Method (τ -MVM) [34,35] to predict the lifetime of metallic materials subjected to VA fretting fatigue loading.

2. The τ -MVM: stress components relative to the critical plane

The fretting fatigue design technique proposed in the present investigation is based on the use of the MWCM [32,33]. The MWCM is a critical plane approach that estimates fatigue damage through the normal and shear stress components relative to the plane of maximum shear stress amplitude (i.e., the critical plane). Accordingly, the present section reviews the definitions that are used to estimate the critical plane

stress components of interest. The definitions reported in what follows were derived by taking advantage of the τ -MVM [34,35].

Consider a body subjected to a system of time-variable forces and moments that result in a time-dependent three-dimensional state of stress, $[\sigma(t)]$, at the sub-surface point of interest (point O in Fig. 1a). Given stress tensor $[\sigma(t)]$, the τ -MVM [34,36] postulates that the critical plane is that material plane which contains the direction, MV, associated with the maximum variance of the resolved shear stress, $\tau_{MV}(t)$ (Fig. 1b). Since variance is a statistical measure of dispersion that stands independently of the characteristics of the data sample being considered, the

τ -MVM can be used both with CA and VA load histories. Accordingly, under CA as well as under VA fatigue loading, the first step is to post-process stress tensor $[\sigma(t)]$ at point O so that the orientation of that material plane containing the direction experiencing the maximum variance of the resolved shear stress can be determined unambiguously [34]. As soon as the orientation of the critical plane is known, tensor $[\sigma(t)]$ is projected along the direction perpendicular to the critical plane itself to determine normal stress $\sigma_n(t)$.

If the body seen in Fig. 1a is subjected to a CA load history, the amplitude, τ_a , and the mean value, τ_m , of the shear stress relative to the

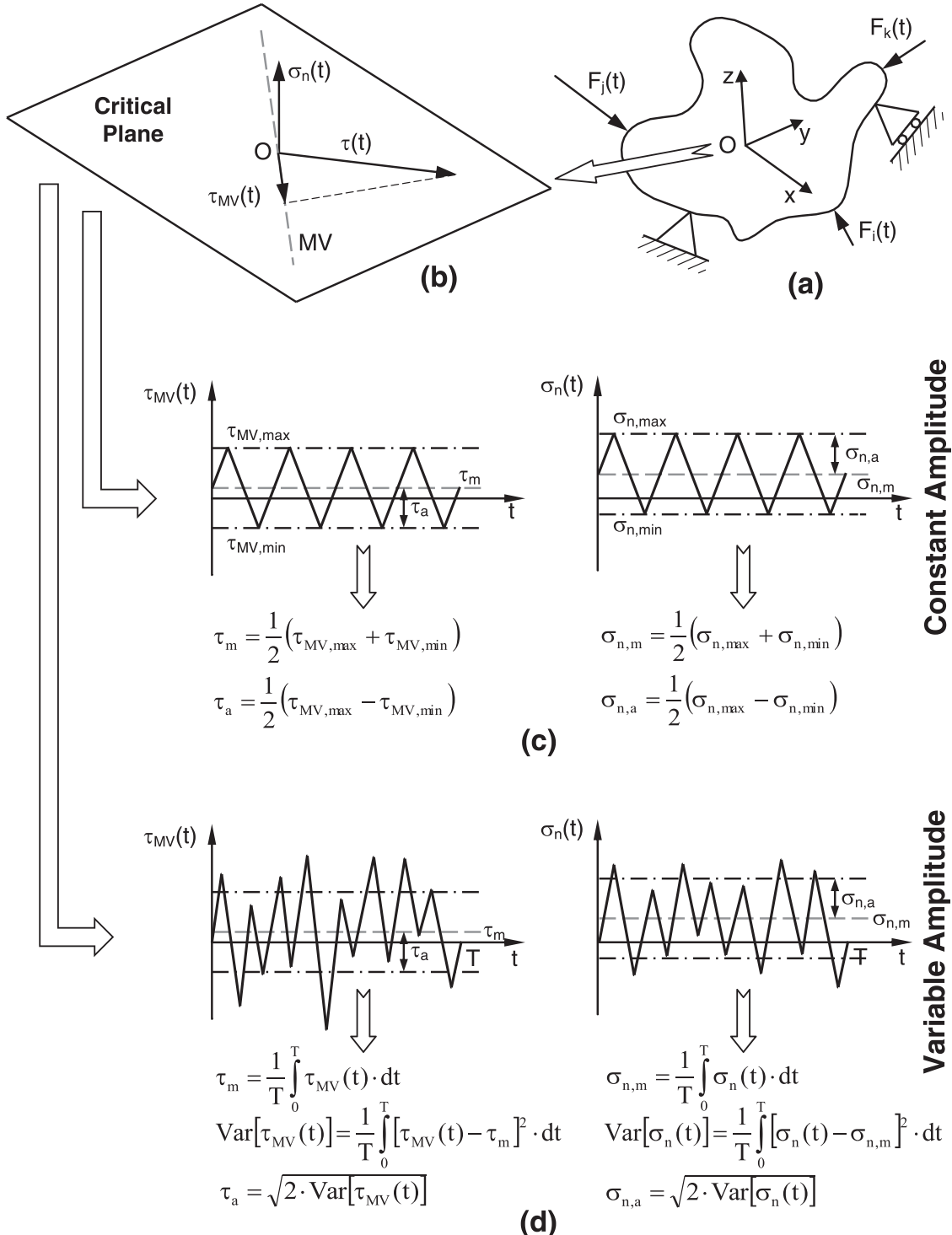


Fig. 1. Stress quantities relative to the critical plane determined according to the τ -MVM under constant (c) and variable (d) amplitude fatigue loading.

critical plane take on the following values (Fig. 1c):

$$\tau_a = \frac{1}{2} (\tau_{MV,max} - \tau_{MV,min}) \quad (1)$$

$$\tau_m = \frac{1}{2} (\tau_{MV,max} + \tau_{MV,min}) \quad (2)$$

Correspondingly, the amplitude, $\sigma_{n,a}$, and the mean value, $\sigma_{n,m}$, of normal stress $\sigma_n(t)$ are calculated as follows (Fig. 1c):

$$\sigma_{n,a} = \frac{1}{2} (\sigma_{n,max} - \sigma_{n,min}) \quad (3)$$

$$\sigma_{n,m} = \frac{1}{2} (\sigma_{n,max} + \sigma_{n,min}) \quad (4)$$

In Eqs. (1) to (4) the subscripts max and min are used to denote the maximum and minimum value, respectively, of the stress signal under consideration.

If the body sketched in Fig. 1a is subjected to a VA load history defined over the time interval [0, T], the mean value and the equivalent amplitude of the shear and normal stress relative to the critical plane (at point O) are calculated via the following definitions [37,38]:

$$\tau_m = \frac{1}{T} \int_0^T \tau_{MV}(t) \bullet dt \quad (5)$$

$$\tau_a = \sqrt{2 \bullet \text{Var}[\tau_{MV}(t)]} \text{ where } \text{Var}[\tau_{MV}(t)] = \frac{1}{T} \int_0^T [\tau_{MV}(t) - \tau_m]^2 \bullet dt \quad (6)$$

$$\sigma_{n,m} = \frac{1}{T} \int_0^T \sigma_n(t) \bullet dt \quad (7)$$

$$\sigma_{n,a} = \sqrt{2 \bullet \text{Var}[\sigma_n(t)]} \text{ where } \text{Var}[\sigma_n(t)] = \frac{1}{T} \int_0^T [\sigma_n(t) - \sigma_{n,m}]^2 \bullet dt \quad (8)$$

Fig. 1d explains graphically the meaning of definitions (5) to (8). This figure shows that, since their calculation is based on the variance concept, both τ_a and $\sigma_{n,a}$ are proportional to the amount of variation of stress signals $\tau_{MV}(t)$ and $\sigma_n(t)$, respectively.

3. Fatigue damage according to the modified Wöhler curve method

The way the MWCM quantifies fatigue damage is conceptualised through the modified Wöhler diagram seen in Fig. 2. This log-log chart plots the maximum shear stress amplitude on the critical plane, τ_a , against the number of cycles to failure, N_f . The MWCM assesses the extent of damage based on the effective value of the critical plane stress

ratio which is defined as [39,40]:

$$\rho_{eff} = \frac{m \bullet \sigma_{n,m} + \sigma_{n,a}}{\tau_a} \quad (9)$$

In definition (9) the mean stress sensitivity index, m, quantifies the material sensitivity to the presence of non-zero mean stresses normal to the critical plane. The value of material fatigue constant m varies in the range 0–1 and is determined experimentally from a fatigue curve generated under a load ratio $R = \sigma_{min}/\sigma_{max}$ larger than – 1 [40]. Thanks to the way it is defined, ρ_{eff} varies not only with the magnitude of the mean stresses [39], but also as the degree of multiaxiality and non-proportionality of the load history being post-processed change [40].

For a specific metallic material, the uniaxial and torsional plain fatigue curve (both determined under a load ratio, R, equal to –1) can be plotted together in the same diagram. This can be done because, while negative inverse slopes k (uniaxial loading, $\rho_{eff}=1$) and k_0 (torsion, $\rho_{eff}=0$) do not vary, the corresponding endurance limits can directly be rewritten as [32,33] (Fig. 2):

$$\tau_{A,Ref}(\rho_{eff} = 1) = \frac{\sigma_A}{2} \quad (10)$$

$$\tau_{A,Ref}(\rho_{eff} = 0) = \tau_A \quad (11)$$

where σ_A and τ_A are the uniaxial and torsional fully-reversed endurance limit, respectively, extrapolated at N_A cycles to failure.

As per the schematic chart of Fig. 2, much experimental evidence confirms that, given this specific way of conceptualising fatigue damage, the torsional fatigue curve ($\rho_{eff}=0$) is always above the uniaxial fatigue curve ($\rho_{eff}=1$) [32,33,40]. Accordingly, the hypothesis can be formed that, for a given material, endurance limit $\tau_{A,Ref}(\rho_{eff})$ decreases as the critical plane stress ratio, ρ_{eff} , increases. Since, for a given material, the available fatigue results that can be used for calibration purposes are, in general, those obtained under uniaxial ($\rho_{eff}=1$) and torsional ($\rho_{eff}=0$) fully-reversed fatigue loading, the modified Wöhler curves for values of ρ_{eff} different from either 0 or 1 must be estimated. This can be done by defining the values of the negative inverse slope, $k_\tau(\rho_{eff})$, and the endurance limit, $\tau_{A,Ref}(\rho_{eff})$, characterising the modified Wöhler curve of interest from the following calibration relationships [33,39,40]:

$$k_\tau(\rho_{eff}) = (k - k_0) \bullet \rho_{eff} + k_0 \text{ for } \rho_{eff} \leq \rho_{lim} \quad (12a)$$

$$k_\tau(\rho_{eff}) = (k - k_0) \bullet \rho_{lim} + k_0 \text{ for } \rho_{eff} > \rho_{lim} \quad (12b)$$

$$\tau_{A,Ref}(\rho_{eff}) = \left(\frac{\sigma_A}{2} - \tau_A\right) \bullet \rho_{eff} + \tau_A \text{ for } \rho_{eff} \leq \rho_{lim} \quad (13a)$$

$$\tau_{A,Ref}(\rho_{eff}) = \left(\frac{\sigma_A}{2} - \tau_A\right) \bullet \rho_{lim} + \tau_A \text{ for } \rho_{eff} > \rho_{lim} \quad (13b)$$

where ρ_{lim} takes on the following value [39,40]:

$$\rho_{lim} = \frac{\tau_A}{2\tau_A - \sigma_A} \quad (14)$$

Within the MWCM theoretical framework, the limit value of the critical plane stress ratio, ρ_{lim} , is used to model the fact that, in the presence of large values of ratio ρ_{eff} , fatigue damage no longer depends solely on the shear stress amplitude relative to the critical plane [41,42]. Therefore, when in Eq. (9) the numerator (that quantifies the effect of the normal stress) becomes significantly larger than the denominator (i. e., τ_a), the conventional critical plane approach must be adapted to take into account the fact that, under these circumstances, the physical processes leading to final breakage change [42]. In the MWCM setting, this is done by shifting from Eqs. (12a) and (13a) to Eqs. (12b) and (13b) [39].

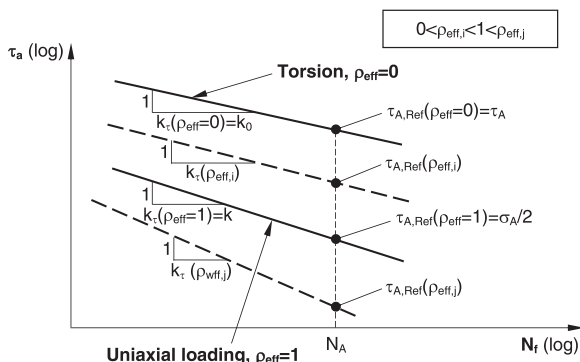


Fig. 2. Modified Wöhler diagram.

4. The fretting fatigue life estimation technique

The fretting fatigue assessment methodology formulated and validated in what follows is based on the use of three distinct ingredients, i. e.: the MWCM, the τ -MVM and the PM. As far as fretting fatigue is concerned, the TCD employed in the form of the PM is used to take into account the effect of the gradients characterising the distribution of the stress in the fretted region. The MWCM instead is used to quantify the extent of damage associated with the degree of multiaxiality and non-proportionality of the local linear-elastic stress fields. Further, via ρ_{eff} this criterion assesses also the detrimental effect of superimposed static normal stresses (i.e., mean stress effect in fatigue). Finally, the τ -MVM is used to calculate the stress quantities of interest, with this being done by taking full advantage of the maximum variance concept. In what follows, these three key ingredients will be combined together to formalise a novel design approach suitable for estimating fretting fatigue lifetime in the presence of CA (Section 4.1) as well as of VA (Section 4.2) load histories.

4.1. Fretting fatigue assessment under constant amplitude loading

The process flow diagrams of Figs. 3 and 4 visualise the design procedure that is recommended to be followed to predict fretting fatigue lifetime under CA time-variable loading [43]. For the sake of clarity, consider then a flat specimen which is subjected to CA axial cyclic stress $\sigma_b(t)$ - resulting from axial cyclic force $F(t)$. Force $P(t)$ is used to push two fretting pads against the specimen's surfaces, with the two pads being subjected also to an CA oscillatory tangential force, $Q(t)$ (Fig. 3a).

According to Fig. 3a and b, the first step is to determine (either analytically or numerically) the linear-elastic multiaxial stress distribution along the focus path. As far as fretting fatigue is concerned, the focus path is defined as a straight line that originates from the edge of the contact zone in the critical region (point A in Fig. 3b) and is perpendicular to the contact surface itself [15,43].

Having determined the relevant stress fields, the subsequent step is to calibrate the MWCM's governing equations, Eqs. (12a) to (13b), via the parent material uniaxial and torsional fully-reversed fatigue curve.

In order to extend the use of the PM to the medium-cycle fatigue regime, the relevant critical distance for the material under investigation is expressed as follows [44,45]:

$$L_M(N_f) = A \cdot N_f^B \quad (15)$$

According to definition (15), for a given material, length scale $L_M(N_f)$

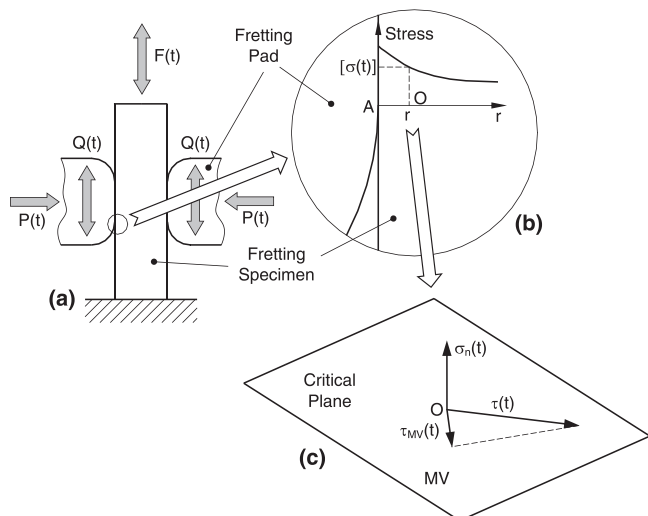


Fig. 3. The τ -MVM applied in conjunction with the PM to estimate, along the focus path, the stress components relative to the critical plane.

is assumed to increase as the number of cycles to failure decreases [44]. This assumption takes as its starting point the idea that, in the presence of a stress concentrator, the size of the fatigue process zone increases as magnitude of the applied loading increases. Since the TCD critical distance is linked with the size of the process zone [7,39], it is logical to hypothesise that length scale $L_M(N_f)$ increases as N_f decreases. A and B are material constants that can directly be determined by post-processing the fatigue results generated by testing (under $R=-1$) both plain specimens and samples weakened by a known geometrical feature [40,44,45]. The procedure suggested as being followed to estimate constants A and B will be reviewed thoroughly in Section 6.2.

As soon as relationships $k_\tau(\rho_{eff})$, $\tau_{A,Ref}(\rho_{eff})$ and $L_M(N_f)$ are calibrated, fretting fatigue lifetime can be predicted using the recursive strategy outlined in Figs. 3 and 4. The first step is to use the τ -MVM to determine, along the focus path, the orientation of the critical plane and the associated stress quantities at any distance r from the edge of the contact zone in the critical region (Figs. 3c, 4a and 4b). For a given value of distance r , stress quantities τ_a , Eq. (1), $\sigma_{n,a}$, Eq. (3), and $\sigma_{n,m}$, Eq. (4), are then used to estimate ρ_{eff} , Eq. (9) – Fig. 4a–c. The calculated value for stress ratio ρ_{eff} allows the MWCM's governing equations to be calibrated unambiguously (Fig. 4d). At this point, the modified Wöhler curve being estimated is used to predict the number of cycles to failure, N_f , via the following standard power law (Fig. 4d):

$$N_f = N_A \cdot \left[\frac{\tau_{A,ref}(\rho_{eff})}{\tau_a} \right]^{k_\tau(\rho_{eff})} \quad (16)$$

Subsequently, N_f estimated at a distance from the edge of the contact zone equal to r is used to determine, via Eq. (15), the corresponding critical length, $L_M(N_f)$. Following this procedure, N_f and the associated critical distance can be calculated at any point along the focus path. The fretted component being designed is then assumed to fail at the number of cycles to failure equal to $N_{f,e}$, where $N_{f,e}$ is the number of cycles to failure that satisfies the following PM-related mathematical condition [37,43,44] (Fig. 4e):

$$\frac{L_M(N_{f,e})}{2} = r \quad (17)$$

The approach summarised in Figs. 3 and 4 can be used in situations of practical interest by coding a recursive procedure suitable for reaching convergence by making distance r vary (Fig. 4e).

Having summarised the procedure we propose to estimate fretting fatigue lifetime under CA loading, it is worth considering in detail the definition that is recommended to be used to determine the orientation of the focus path (Fig. 3b). The physical model behind this definition takes as a starting point the idea that damage under fatigue loading is the result of a number of processes taking place, near the crack initiation location, in a finite size region [40,46,47]. According to the TCD used in form of the Volume Method, the size of this reference volume approaches $L(N_f)$ [7,48]. Therefore, as per Eq. (15), the size of the process zone decreases as the number of cycles to failure increases. In terms of fatigue assessment, the TCD Volume Method makes use of an effective stress that is calculated by averaging the linear-elastic stress over the process zone itself [7,48]. However, the effective stress estimated according to the Volume Method is the same as the one determined (according to the PM) at a distance from the crack initiation point equal to $L(N_f)/2$ [7,44]. Based on this equivalence in terms of effective stress, it is reasonable to form the hypothesis that, according to the PM, the focus path as defined in Fig. 3b represents the set of those material points whose stress state is proportional to the extent of fatigue damage that is accumulated in the material within the process zone. In other words, since the size of the structural volume increases as the number of cycles to failure decreases, the point at the centre of the structural volume (whose stress state is used to estimate fatigue damage according to the PM) increases its distance from the crack initiation site as N_f decreases. Thus, as the PM reference point moves away from the assumed crack

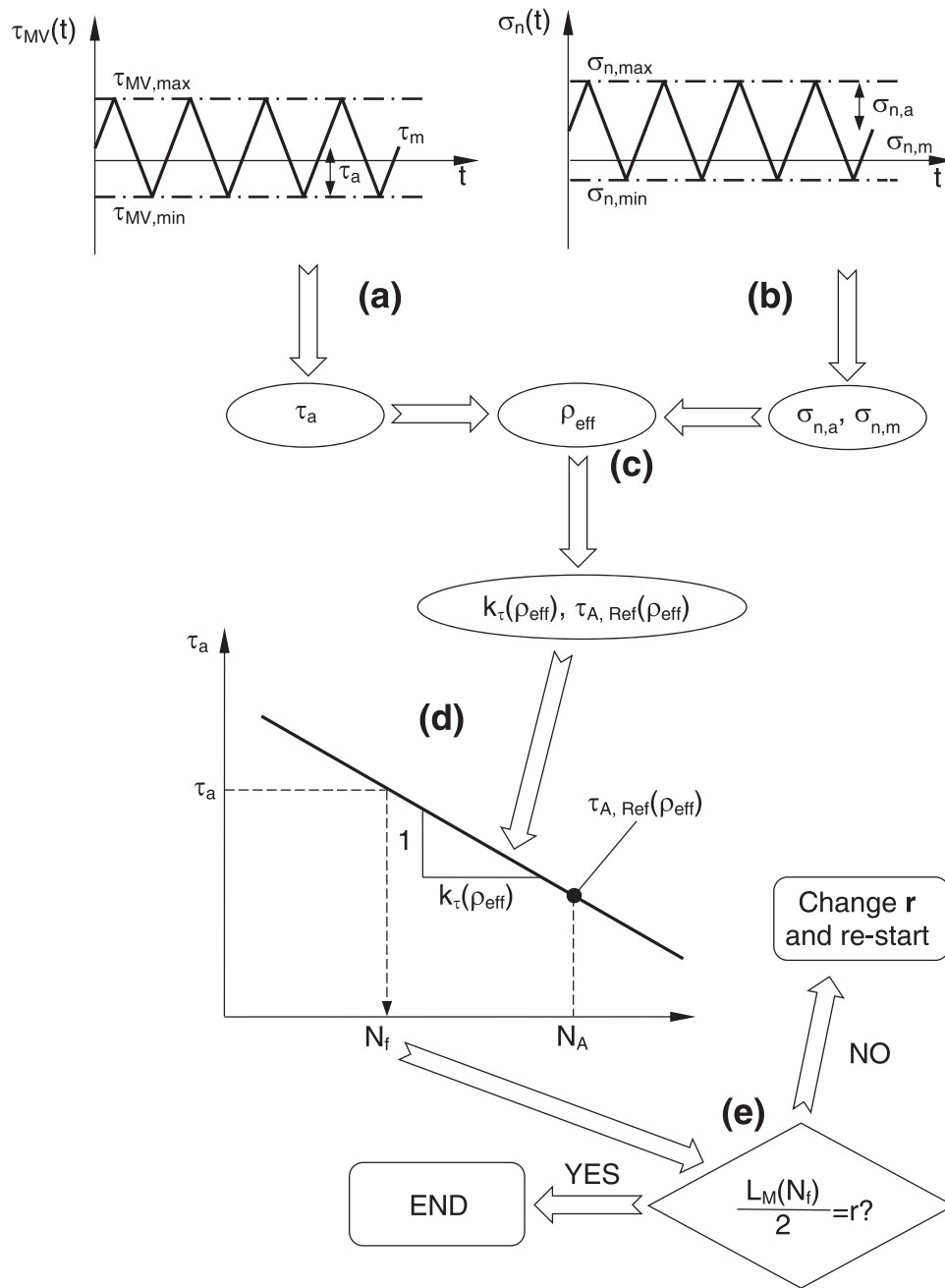


Fig. 4. The MWCM applied in conjunction with the PM and the τ -MVM to estimate lifetime under CA fretting fatigue loading.

initiation point, it draws a straight line that is nothing but the focus path as defined in Fig. 3b [45]. The reasoning behind the definition of the focus path applies independently of the complexity of the loading history being assessed [37]. Accordingly, the same definition will be adopted also in the next section to extend the use of the proposed fretting fatigue design methodology to VA situations.

4.2. Fretting fatigue assessment under variable amplitude loading

The procedure being proposed here to estimate VA fretting fatigue lifetime is summarised via the flowcharts reported in Figs. 3 and 5. For the sake of simplicity, consider again the case of a flat specimen and two fretting pads (Fig. 3a). In this instance the applied forces and stresses are supposed to vary randomly over the time interval $[0, T]$.

As in the CA case, the focus path is taken coincident with a straight line that emanates from the edge of the contact zone in the critical region

(point A in Fig. 3b) and is normal to the contact surface [15,43].

Assume now that the point of interest along the focus path (i.e., point O in Fig. 3b) is at a distance from the edge of the contact zone equal to r . The linear-elastic stress tensor, $[\sigma(t)]$, at point O is then post-processed according to the τ -MVM to identify that material plane containing the direction which experiences the maximum variance of the resolved shear stress (direction MV in Fig. 3c) [34]. As soon as the orientation of the critical plane is known, the associated shear stress amplitude, τ_a , is determined according to definition (6) – Fig. 5a. Similarly, the mean value, $\sigma_{n,m}$, and the amplitude, $\sigma_{n,a}$, of the stress normal to the critical plane are calculated using definitions (7) and (8), respectively – Fig. 5b.

Stress components τ_a , $\sigma_{n,m}$ and $\sigma_{n,a}$ allow the degree of multiaxiality and non-proportionality of the stress state at point O as well as the effect of non-zero mean stresses to be quantified directly via ratio ρ_{eff} (Fig. 5c), Eq. (9). The calculated value for ρ_{eff} is then used to estimate the corresponding modified Wöhler curve from Eqs. (12a) to (13b) that are

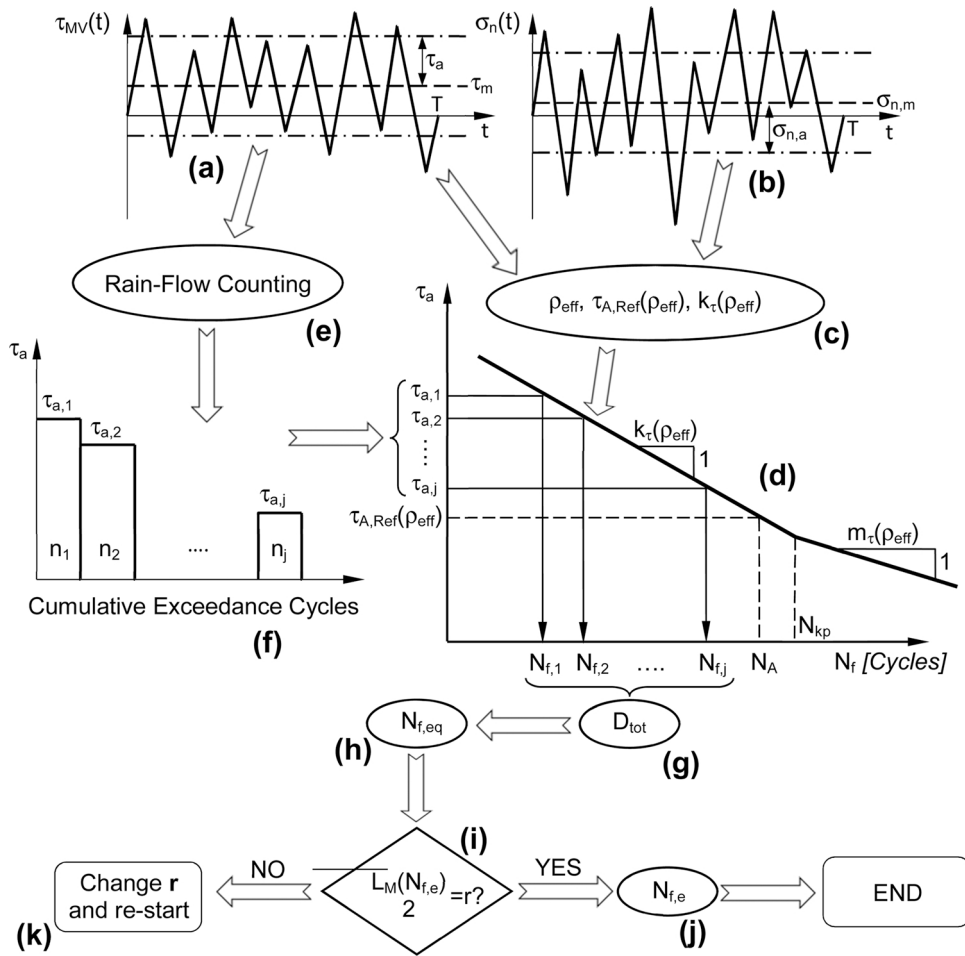


Fig. 5. The MWCM applied in conjunction with the PM and the τ -MVM to estimate lifetime under VA fretting fatigue loading.

calibrated through the parent material uniaxial and torsional fully-reversed CA fatigue curve (Figs. 5c and 5d).

To assess the damaging effect of those cycles of low shear stress amplitude in a more effective, accurate way, the negative inverse slope in the high-cycle fatigue regime is recommended to be adjusted as follows [37,49] (Fig. 5d):

$$m_{\tau}(\rho_{\text{eff}}) = 2 \bullet k_{\tau}(\rho_{\text{eff}}) - 1 \text{ for } \rho_{\text{eff}} \leq \rho_{\text{lim}} \quad (18a)$$

$$m_{\tau}(\rho_{\text{eff}}) = 2 \bullet k_{\tau}(\rho_{\text{lim}}) - 1 = \text{const for } \rho_{\text{eff}} > \rho_{\text{lim}} \quad (18b)$$

As to the above correction, in rigorous terms, the position of the knee point (N_{kp} in Fig. 5d) should be determined by running appropriate experiments. If this is not possible, its position can be assumed according to the available recommendations [50].

By taking advantage of the long-established rainflow counting method [51,52], stress signal $\tau_{MV}(t)$ is post-processed to count the shear stress cycles (Figs. 5a and 5e). It is important to point out here that the rainflow counting method can be used in a rigorous, standard way since, by its definition, $\tau_{MV}(t)$ is always a unidimensional stress quantity (with this holding true independently of the degree of multiaxiality characterising the assessed state of stress).

The resulting load spectrum (Fig. 5f) is then used together with the relevant modified Wöhler curve (Fig. 5d) to quantify the damage content associated with any shear stress cycle being counted so that the resulting total damage is estimated as follows (Fig. 5g):

$$D_{\text{tot}} = \sum_{i=1}^j \frac{n_i}{N_{f,i}} \quad (19)$$

As soon as total damage D_{tot} is known, it is used to calculate an equivalent number of cycles to failure, $N_{f,\text{eq}}$, via the following relationship [37] (Fig. 5h):

$$N_{f,\text{eq}} = \frac{\sum_{i=1}^j n_i}{\sum_{i=1}^j \frac{n_i}{N_{f,i}}} \quad (20)$$

so that critical distance $L_M(N_f)$, Eq. (15), can be rewritten as [37]:

$$L_M(N_{f,\text{eq}}) = A \bullet N_{f,\text{eq}}^B = A \bullet \left(\frac{\sum_{i=1}^j n_i}{\sum_{i=1}^j \frac{n_i}{N_{f,i}}} \right)^B \quad (21)$$

It is important to point out here that in Eq. (21) constants A and B are still estimated for the material under investigation from two sets of fatigue results generated by testing (under CA R=-1) both plain samples and specimens containing a known geometrical feature [40,44,45].

If the critical distance value determined through Eq. (21) satisfies the following PM-related condition (Fig. 5i):

$$\frac{L_M(N_{f,\text{eq}})}{2} = r \quad (22)$$

where r is the distance, measured along the focus path, from the edge of the contact zone (point A in Fig. 3), then the number of cycles to failure, $N_{f,e}$, is predicted using the following relationship [37] (Fig. 5j):

$$N_{f,e} = \frac{D_{cr}(\rho_{eff}) \cdot n_{tot}}{D_{tot}} = \frac{D_{cr}(\rho_{eff}) \cdot \sum_{i=1}^j n_i}{\sum_{i=1}^j \frac{n_i}{N_{fi}}} \quad (23)$$

In Eq. (23) $D_{cr}(\rho_{eff})$ is the critical value of the damage sum. In the most general case, the hypothesis is formed that $D_{cr}(\rho_{eff})$ varies as the degree of multiaxiality and non-proportionality of the assessed stress state changes [37]. However, the problem can be simplified greatly if the critical value of the damage sum is taken invariably equal to unity as suggested by Palmgren [30] and Miner [31] in their pivotal investigations. Alternatively, $D_{cr}(\rho_{eff})$ can be set equal to 0.27 and to 0.37 for steel and aluminium, respectively, with this resulting in a larger degree of conservatism compared to the one obtained by using Palmgren and Miner's recommended value [53].

Turning back to the VA fretting fatigue assessment methodology summarised in Figs. 3 and 5, if, in contrast, condition (22) is not satisfied (Fig. 5k), then the same procedure as the one described above has to be re-used to estimate $N_{f,e}$ at a different point along the focus path, with this approach being applied recursively until convergence occurs.

5. Materials, methods and experimental results

5.1. Materials and static/fatigue testing

In order to validate the accuracy and reliability of the novel fretting fatigue assessment technique formulated in the previous sections, a comprehensive experimental investigation was carried out at the Structures Laboratory of the University of Sheffield, UK. This experimental work involved the use of two different materials, i.e. grey cast iron (CI) 40054 and grey CI 40060 (controlled carbon).

The static properties of the two materials being investigated were determined by testing 100 mm (width) x 6 mm (thickness) dog-bone flat specimens with a 100 kN Mayes servo-hydraulic axial machine at a displacement rate of 0.0333 m/s. For any iron-carbon alloy being tested, the ultimate tensile strength, σ_{UTS} , Young's modulus, E , and Poisson's ratio, ν , were obtained by averaging the results from three individual tests. This standard experimental procedure returned the following values for CI 40054: σ_{UTS} = 354 MPa, E = 100 GPa and ν = 0.26. Similarly, the relevant static properties for CI 40060 were determined to be: σ_{UTS} = 278 MPa, E = 108 GPa, and ν = 0.25.

The fatigue properties of the iron-carbon alloys under investigation were obtained using a 100 kN Mayes servo-hydraulic machine to test flat specimens under axial loading and a SCHENCK tension-torsion machine (axial load capacity=250 kN; torsion capacity=2.2 kNm) to test cylindrical samples under torsional loading.

The plain material fatigue properties were generated by testing (at 10 Hz under load ratios, R , equal to -1 as well as to 0.1) dog-bone flat specimens having width equal to 10 mm and thickness to 6 mm.

To calibrate the L_M vs. N_f relationship for the two iron-carbon alloys under investigation, the necessary notch fatigue curves were determined by testing flat specimens with opposite edge V-notches. The average dimensions of the specimens of CI 40054 were as follows: gross width equal to 25.7 mm, net width 9.7 mm, thickness 5.9 mm, notch root radius 0.22 mm and notch opening angle to 30° . In contrast, the average dimensions of the specimens of CI 40060 were: gross width equal to 25.6 mm, net width 10.3 mm, thickness 6.1 mm, notch root radius 0.16 mm and notch opening angle 30° .

The fully-reversed torsional fatigue curves for the materials were generated at a frequency of 5 Hz. The solid cylindrical specimens being tested had average gross diameter equal to 14.9 mm and average net diameter equal to 9.9 mm.

The failure criterion being adopted for the axial fatigue tests was the complete separation of the specimens. In contrast, fatigue failures under torsion were defined by 20% stiffness drop. Run-out tests were stopped at $2 \cdot 10^6$ cycles.

The results generated according to the experimental protocol described above are summarised in the stress range vs. number of cycles to failure diagrams reported in Fig. 6. The graphs summarising the results generated by testing the notched specimens are plotted in terms of range of the stress referred to the nominal net area, $\Delta\sigma_{net}$.

The scatter bands plotted in the diagrams of Fig. 6 were determined by assuming a log-normal distribution of the cycles to failure for any stress level, with the confidence being set equal to 95 % [54]. The level of scattering characterising these bands was evaluated in terms of ratio between the endurance limits determined for 10 % and 90 % probability of survival - T_σ for the uniaxial case and T_τ for the torsional case. The results from the statistical reanalyses are reported in Table 1 in terms of endurance limit amplitude (σ_A , σ_{An} or τ_A) at $N_A = 10^6$ cycles to failure, negative inverse slope (k or k_0) and scatter level (T_σ or T_τ).

5.2. Fretting fatigue testing and results

The fretting fatigue results utilised to validate the design approach formulated in Section 4 were generated in the Materials Testing Laboratory of the University of Sheffield using the cruciform hydraulic biaxial machine seen in Fig. 7a. This machine allows two horizontal actuators and two vertical actuators to be controlled independently. Each actuator has a load capacity of 100 kN and a displacement of ± 25 mm. In the fretting fatigue testing configuration, the horizontal actuators are used to apply a CA/VA axial cyclic force to a flat dog-bone specimen (Fig. 7b). The vertical actuators are used instead to push (either statically or cyclically) two fretting pads against the flat specimens. Accordingly, the static/time-variable forces applied to run the fretting fatigue tests are controlled both along a horizontal direction and along a vertical direction. Since the two vertical actuators are equipped with two independent loading cells, the controller is capable of detecting variation in the contact arrangement between each pad and the associated fretted surface.

The machine is designed so that both the fretting pads and the specimens can be removed and replaced, with this allowing new pads to be used for each individual test being run.

In terms of testing set-up, specimens and pads were aligned by simply using standard gauge blocks/reference plates that were directly attached to the frame of the testing machine.

Before implementing the planned campaign of experiments, the accuracy and reliability of our fretting fatigue testing rig was checked extensively using specific instrumented specimens and pads that were equipped with a series of strain gauges. In particular, according to Fig. 7c, a set of strain gauges was attached to the lateral surfaces of the calibration specimens, whereas a second set of specimens was attached to the two flat faces of the upper part of the instrumented pads. The calibration constants linking, via a simple linear relationship, the magnitude of applied force with the resulting local strains were determined by using a standard axial testing machine. The calibration constants for the specimens were determined both under tension and under compression, with the constant for the instrumented pads being determined solely under compression. The strain gauges attached to the lateral surfaces of the dog-bone specimens and those attached to the pads were used to assess the machine's accuracy and reliability in controlling the horizontal and vertical actuators, respectively. This standard validation procedure allowed us to compare systematically the feedback signals used by the controller of the testing machine with the corresponding information gathered via the strain gauges attached to the calibration specimens as well as to the calibration pads.

The fretting fatigue results of interest were generated by testing dog-bone flat specimens having, in the gauge region, thickness equal to 9 mm and width to 10 mm. Two batches of samples were machined using CI 40054 and CI 40060, respectively.

The fretting cylindrical pads being used were made of either CI 40054 or steel, with the steel being coated with zinc phosphate. The pads had thickness equal to 12 mm, height equal to 15 mm, length equal

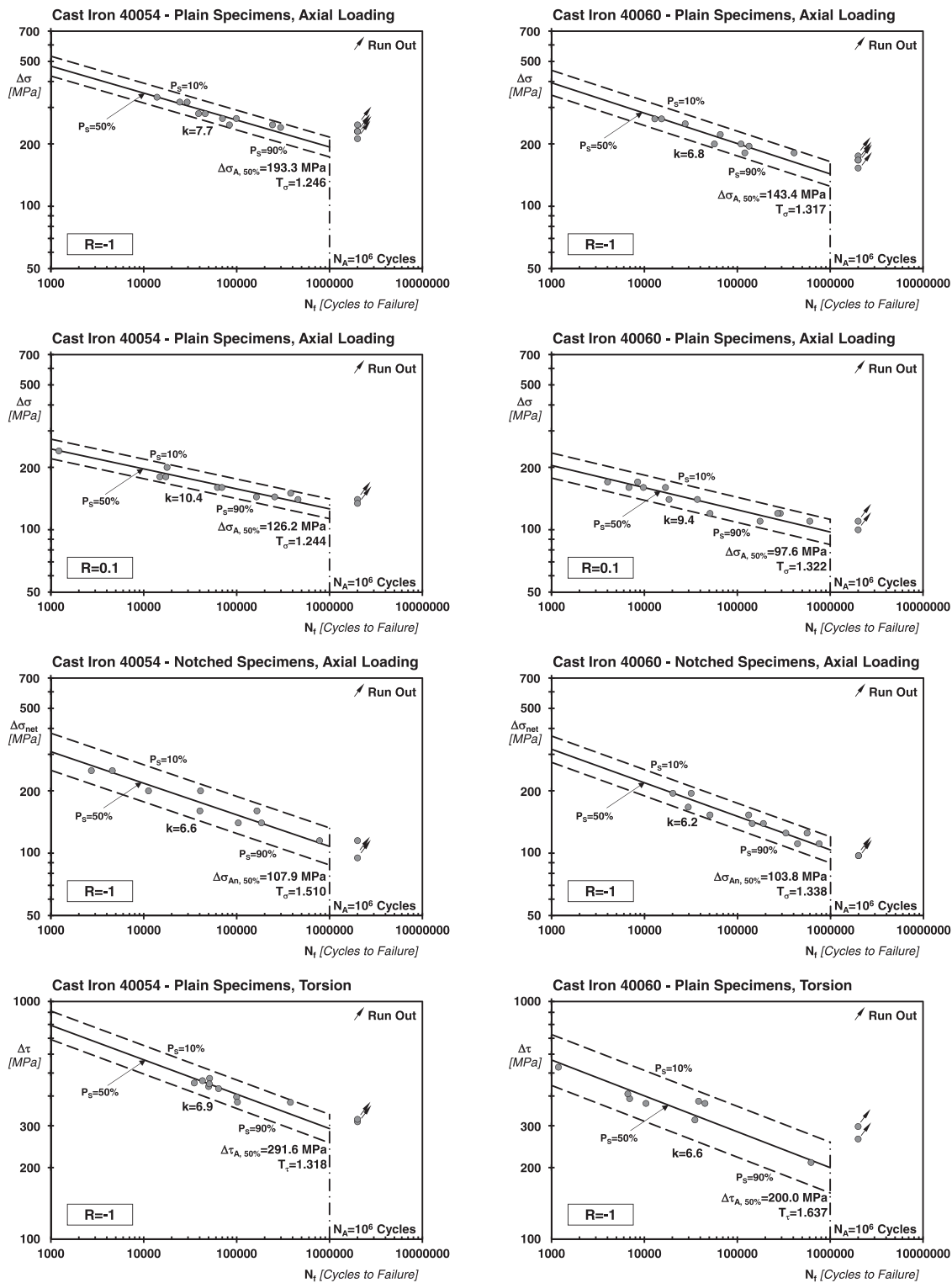


Fig. 6. Fatigue results generated under axial loading and torsion by testing plain and notched specimens of Cast Iron 40054 and of Cast Iron 40,060.

to 40 mm and contact radius, R_p equal to either 20 mm, 75 mm or 100 mm. Intentionally, the pads were larger than the width of the specimens. This allowed us to have a more uniform distribution of the stress in the contact region during testing, with this minimising the effect of potential stress concentration phenomena occurring at the lateral surfaces.

To generate the results under CA fretting fatigue loading, each individual specimen was first clamped using the two mechanical grips

attached to the horizontal actuators. Subsequently, the two cylindrical pads were pushed against the specimen by applying a normal load, $P(t)$. During CA testing, this normal load was either kept constant or varied sinusoidally. A CA sinusoidal load $F(t)$ (characterised by a load ratio, R , equal to either -1 or 0.1) was then applied to one end of the specimens, while the other end was kept fixed in displacement control. Sinusoidal force $F(t)$ was applied at a frequency of 10 Hz. In those tests run by making normal load vary over time, force signals $P(t)$ and $F(t)$ were in-

Table 1

Summary of the experimental results generated under axial loading and torsion by testing plain and notched specimens of CI 40054 and of CI 40060.

Material	Load type	Specimen type	Number of tests	R	$\frac{\sigma_A^a, \sigma_{An}^{a,b}}{[MPa]}$	$\frac{\tau_A^a}{[MPa]}$	k	k_0	T_σ	T_τ
Cast Iron 40054	Axial	Plain	14	-1	96.6		7.7		1.246	
	Axial	Plain	12	0.1	63.1		10.4		1.244	
	Axial	Notched	11	-1	54.0		6.6		1.510	
	Torsion	Plain	11	-1		145.8		6.9		1.318
Cast Iron 40060	Axial	Plain	13	-1	71.7		6.8		1.317	
	Axial	Plain	14	0.1	48.8		9.4		1.322	
	Axial	Notched	13	-1	51.9		6.2		1.338	
	Torsion	Plain	10	-1		100.0		6.6		1.637

^a Endurance limit amplitude extrapolated at $N_A=10^6$ cycles to failure^b Endurance limit amplitude referred to the nominal net area

phase. The failure criterion adopted to define the number of cycles to failure, N_f , was the complete separation of the specimens.

The results generated under CA fretting fatigue loading are summarised in Table 2 in terms of: specimen material; pad material; pad radius, R_p ; amplitude, P_a , and mean value, P_m , of sinusoidal normal force $P(t)$; amplitude, F_a , and mean value, F_m , of sinusoidal axial force $F(t)$; and experimental number of cycles to failure, N_f .

The results under VA fretting fatigue loading were generated by pushing the two cylindrical pads against the fretting specimen by a static normal load, P_m . A VA sinusoidal load signal, $F(t)$, was then applied (at a frequency of 10 Hz) to one end of the sample, with the other end being kept fixed. The two VA load histories used in the present investigation are summarised in Table 3 in terms of ratio between the force amplitude characterising the i -th stress level, $F_{a,i}$, and the maximum amplitude of the force in the spectrum, $F_{a,max}$. Further, Table 3 reports also the number of cycles, n_i , associated with any stress level forming the two spectra considered. Load spectrum A had a length, $L_S = \sum n_i$, equal to 50 cycles and it was applied exploring load ratios equal to both -1 and 0 . Load spectrum B instead had L_S equal to 40 cycles and it was applied by setting the load ratio invariably equal to -1 . All the experimental results under VA fretting fatigue loading were generated by applying the cycles in random order, with the adopted failure criterion being again the complete breakage of the specimens.

The experimental results generated under VA fretting fatigue loading are summarised in Table 4 in terms of: specimen material; pad material; pad radius, R_p ; load spectrum; static value of the normal force, P_m ; maximum amplitude of the axial force, $F_{a,max}$, in the load history; load ratio characterising the applied VA load spectrum, R ; and experimental number of blocks to failure, N_b .

It is worth concluding by observing that inspection of the fracture surfaces revealed that, as expected, the vast majority of the fatigue cracks initiated at the edge of the contact zone. This observation held true under both CA and VA fretting fatigue loading. Fig. 7d shows four representative examples of the typical cracking behaviour displayed by the tested iron-carbon alloys.

6. Validation

6.1. Estimation of the constants in the MWCM's governing equations

To assess the accuracy of the proposed fretting fatigue design methodology against the experimental results listed in Tables 2 and 4, the first step was to calibrate the MWCM governing equations. To this end, Eqs. (12a) to (13b) were calibrated via the plain fully-reversed endurance limits (extrapolated at $N_A=10^6$ cycles to failure) and the corresponding negative inverse slopes listed in Table 1.

The plain material fully reversed endurance limits were used also to estimate the limit value of the effective critical plane stress ratio, ρ_{lim} . Since, according to Eq. (14), ρ_{lim} was calculated to be slightly lower than unity, as recommended in Ref. [55], it was set equal to unity for both CI 40054 and CI 40060.

The plain fatigue curves determined under a load ratio equal to 0.1 (see Table 1) were employed to calculate the mean stress sensitivity index, m , for the two materials under investigation. In particular, m was estimated via the following relationship [40,45]:

$$m = \frac{\tau_a^*}{\sigma_{n,m}^*} \left(2 \bullet \frac{\tau_A - \tau_a^*}{2\tau_A - \sigma_A} - \frac{\sigma_{n,a}^*}{\tau_a^*} \right) \quad (24)$$

where τ_a^* , $\sigma_{n,m}^*$, and $\sigma_{n,a}^*$ are the stress components relative to the critical plane at the endurance limit condition [40]. This simple calculation returned a mean stress sensitivity index equal to 0.141 for CI 40054 and to 0.146 for CI 40060.

Finally, the MWCM was applied to post-process the results generated under VA fretting fatigue loading by correcting the design curve in the high-cycle fatigue regime using Eqs. (18a) and (18b), with N_{kp} being taken equal to 10^7 cycles to failure.

6.2. Estimation of the constants in the L_M vs N_f relationship

The sketches of Fig. 8 explain the procedure that was used to estimate, for the two materials under investigation, constants A and B in the critical distance vs. number of cycles to failure relationship, Eq. (15) [40, 44]. According to Fig. 8 material fatigue constants A and B can directly be estimated from the plain fatigue curve and from a fatigue curve determined experimentally by using specimens weakened by a notch having known profile. In this context, it is worth recalling here that experimental evidence suggests that the notch fatigue curve used to calibrate function $L_M(N_f)$ should be generated by testing specimens containing notches that are as sharp as possible [56].

Turning back to Fig. 8, initially attention can be focused on a specific number of cycles to failure, i.e. N_f^* in Fig. 8a. According to the schematic Wöhler diagram of Fig. 8a, the range of the stress cracking the unnotched material at N_f^* cycles to failure is equal to $\Delta\sigma$. In a similar way, by focusing attention on the notch fatigue curve it is straightforward to estimate the range of the nominal stress, $\Delta\sigma_{net}$, resulting in a fatigue failure again at N_f^* cycles to failure. Given the notched geometry under investigation, the linear-elastic stress field along the notch bisector can be determined either numerically or analytically, where this stress field is to be estimated by setting the nominal stress equal to $\Delta\sigma_{net}$ (Fig. 8b). According to the PM [7], the distance from the notch tip at which the range of the linear-elastic stress is equal to the stress range, $\Delta\sigma$, breaking the unnotched material at N_f^* cycles to failure is equal to $L_M(N_f)/2$ (Fig. 8b). Based on this simple procedure, the critical distance value can then be estimated for different values of N_f^* so that constants A and B in Eq. (15) can be determined unambiguously.

The procedure briefly describe above was used to determine constants A and B for the two iron-carbon alloys under investigation, with this being done by taking advantage of the plain and notch fully-reversed uniaxial fatigue curves reported in Fig. 6. To this end, the relevant linear-elastic stress fields in the notched specimens were determined numerically using commercial Finite Element (FE) code

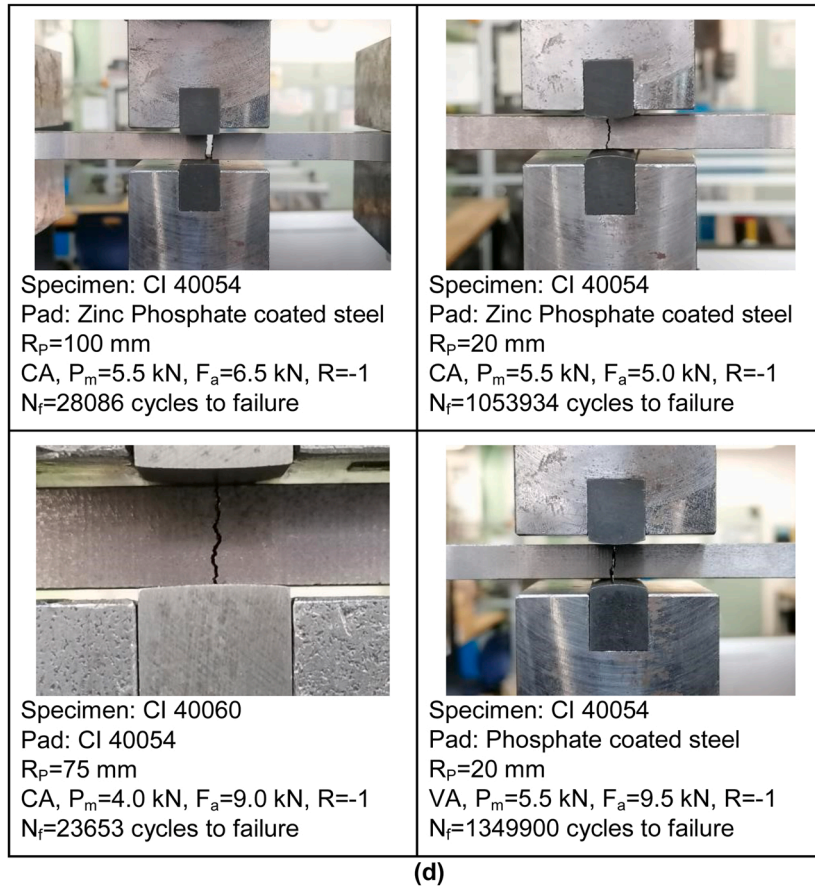
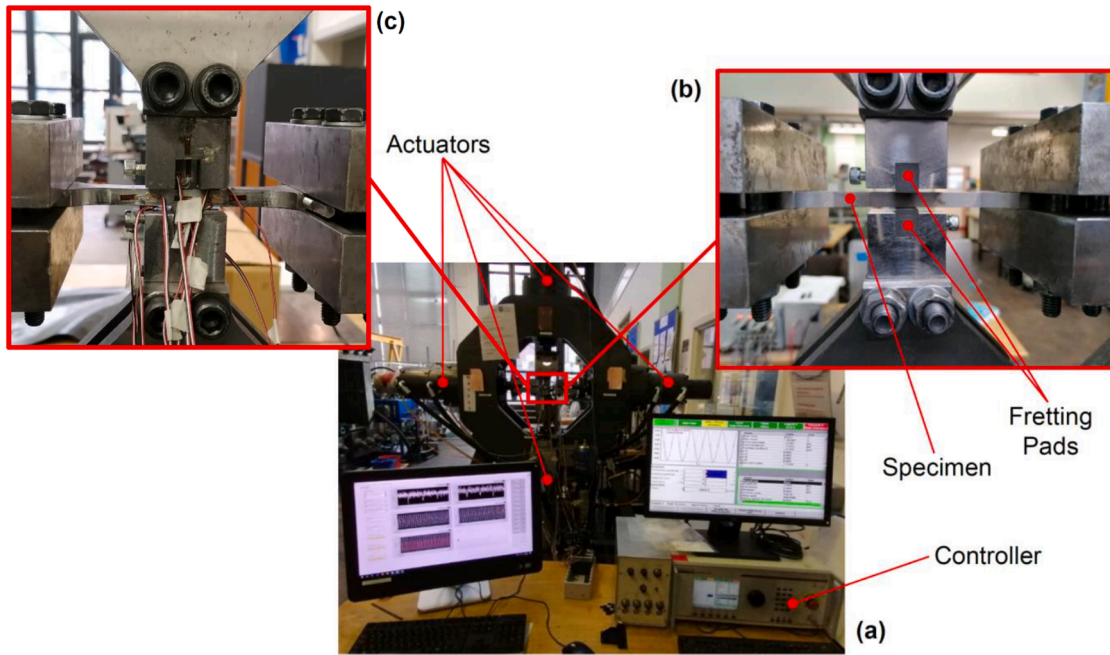


Fig. 7. Fretting fatigue test rig (a); specimen and fretting pads (b); set-up used for the calibration (c); examples of fretting fatigue cracks (d).

Ansys®. In more detail, the notched specimens were modelled using simple 2D linear-elastic elements. The mesh density in the notch region was increased gradually until convergence occurred. This hybrid experimental/numerical approach returned the following values for constants A and B in the L_M vs. N_f relationship:

$$L_M(N_f) = 1.218 \cdot N_f^{-0.042} [\text{mm}] \text{ for } CI40054 \quad (25)$$

$$L_M(N_f) = 1.672 \cdot N_f^{-0.032} [\text{mm}] \text{ for } CI40060 \quad (26)$$

Table 2
Experimental results generated under CA fretting fatigue loading.

Specimen material	Pad material ^a	R_p [mm]	P_a [kN]	P_m [kN]	F_a [kN]	F_m [kN]	N_f [Cycles]
CI 40054	ZPcS	20	0	5.5	8.00	9.78	970,764
CI 40054	ZPcS	20	0	5.5	9.00	11.00	1,107,093
CI 40054	ZPcS	20	0	5.5	9.50	11.61	347,554
CI 40054	ZPcS	20	0	5.5	10.00	12.22	328,400
CI 40054	ZPcS	20	0	5.5	10.50	12.83	368,132
CI 40054	ZPcS	20	0	5.5	11.00	13.44	193,466
CI 40054	ZPcS	20	0	5.5	12.00	14.67	166,731
CI 40054	ZPcS	20	0	5.5	16.00	19.56	86,731
CI 40054	ZPcS	20	0	5.5	7.00	0	32,788
CI 40054	ZPcS	20	0	5.5	6.50	0	86,847
CI 40054	ZPcS	20	0	5.5	6.25	0	130,733
CI 40054	ZPcS	20	0	5.5	6.00	0	547,361
CI 40054	ZPcS	20	0	5.5	5.00	0	1053,934
CI 40054	ZPcS	100	0	5.5	7.00	0	21,619
CI 40054	ZPcS	100	0	5.5	6.50	0	28,086
CI 40054	ZPcS	100	0	5.5	6.25	0	44,523
CI 40054	ZPcS	100	0	5.5	6.00	0	47,932
CI 40054	ZPcS	100	0	5.5	5.50	0	111,079
CI 40054	ZPcS	100	0	5.5	5.00	0	199,438
CI 40054	ZPcS	100	0	5.5	4.75	0	138,909
CI 40060	CI 40054	75	0	5.0	8.00	0	29,670
CI 40060	CI 40054	75	0	5.0	7.00	0	59,770
CI 40060	CI 40054	75	0	5.0	6.50	0	42,985
CI 40060	CI 40054	75	0	4.0	9.00	0	23,653
CI 40060	CI 40054	75	0	3.5	6.25	0	133,335
CI 40060	ZPcS	75	0	4.0	3.50	0	1,703,890
CI 40060	ZPcS	75	0	4.0	4.00	0	1,218,640
CI 40060	ZPcS	75	0	4.0	4.75	0	283,325
CI 40060	ZPcS	75	0	4.0	5.00	0	351,381
CI 40060	ZPcS	75	0	4.0	5.50	0	173,542
CI 40060	ZPcS	75	0	4.0	6.00	0	53,257
CI 40060	CI 40054	75	0.5	4.0	5.50	0	208,500
CI 40060	CI 40054	75	0.5	5.0	6.50	0	65,650
CI 40060	CI 40054	75	0.5	5.0	6.00	0	124,504
CI 40060	CI 40054	75	0.5	5.0	9.50	0	17,788
CI 40060	CI 40054	75	0.5	5.0	7.00	0	52,773
CI 40060	CI 40054	75	1	6.0	7.50	0	50,297
CI 40060	ZPcS	75	0.5	5.0	6.00	0	77,000
CI 40060	ZPcS	75	0.5	5.0	5.50	0	135,000
CI 40060	ZPcS	75	0.5	5.0	5.00	0	338,697
CI 40060	ZPcS	75	0.5	5.0	4.50	0	397,873
CI 40060	ZPcS	75	0.5	5.0	4.00	0	705,000
CI 40060	ZPcS	75	0.5	5.0	4.25	0	561,658
CI 40060	ZPcS	75	0.5	5.0	4.75	0	450,562

^a ZPcS = Zinc Phosphate coated Steel

Table 3
Force amplitude distribution and stepping characterising the adopted load spectra.

Load Spectrum A		Load Spectrum B	
R = -1, 0		R = -1	
$F_{a,i}/F_{a,max}$	n_i [Cycles]	$F_{a,i}/F_{a,max}$	n_i [Cycles]
1	6	1	5
0.9	5	0.9	5
0.8	5	0.8	5
0.7	9	0.7	10
0.6	7	0.6	10
0.5	8	0.5	5
0.4	5		
0.3	5		
L _s = 50 cycles		L _s = 40 cycles	

6.3. Numerical stress analysis

The necessary stress analyses were carried out using FE code Ansys® Workbench by modelling half of the fretting specimen and one pad.

Three specific models were solved, i.e. FE models with pad radius, R_p , equal to 100 mm (CI 40054/coated steel), to 75 mm (CI 40060/CI 40054) and to 20 mm (CI 40054/coated steel). The specimens were modelled using 2D 4-node structural element PLANE182, with the solutions being calculated under a plane strain condition. In particular, the relevant linear-elastic stress fields in the contact region were determined at the mid-section of the specimens by assuming that the associated stress triaxiality was due to a fully-developed plane strain distribution.

As an example, Fig. 9 summarises the numerical procedure followed to determine the relevant local linear-elastic stress fields in the specimens of CI 40054 with a $R_p = 20$ mm pad of zinc phosphate coated steel.

In the models, the height of the pad was taken equal to ten times the contact semi-width to ensure that the boundary conditions applied to the top of the pad itself did not affect the distribution of the pressure [1]. The virtual specimens were constrained to deform along the x-axis, with all the degrees of freedom being constrained for the edge vertical plane on the left-hand side (Fig. 9b). For the pads, the boundary conditions to the vertical lateral surfaces were applied so that the pads could move solely along a vertical direction (Fig. 9c).

The contact region was modelled by defining the contact interface between pad and specimen as “frictional contact pair”. According to the design experience gained at the sponsoring company (www.cummins.

Table 4
Experimental results generated under VA fretting fatigue loading.

Specimen material	Pad material ^a	R_p [mm]	Load Spectrum	P_m [kN]	$F_{n,max}$ [kN]	R	N_b [Blocks]
CI 40054	ZPcS	20	A	5.5	7.50	-1	3223
CI 40054	ZPcS	20	A	5.5	7.00	-1	7516
CI 40054	ZPcS	20	A	5.5	6.50	-1	3384
CI 40054	ZPcS	20	A	5.5	6.25	-1	6480
CI 40054	ZPcS	20	A	5.5	6.00	-1	9525
CI 40054	ZPcS	20	A	5.5	5.75	-1	23,659
CI 40054	ZPcS	20	A	5.5	8.00	0	85,924
CI 40054	ZPcS	20	A	5.5	9.00	0	20,449
CI 40054	ZPcS	20	A	5.5	9.50	0	26,998
CI 40054	ZPcS	20	A	5.5	10.00	0	9180
CI 40054	ZPcS	20	A	5.5	12.00	0	5784
CI 40054	ZPcS	100	A	5.5	5.75	-1	12,503
CI 40054	ZPcS	100	A	5.5	6.00	-1	7223
CI 40054	ZPcS	100	A	5.5	7.00	-1	3699
CI 40054	ZPcS	100	A	5.5	7.50	-1	1712
CI 40054	ZPcS	100	A	5.5	8.00	-1	1060
CI 40054	ZPcS	100	A	5.5	9.00	0	45,281
CI 40054	ZPcS	100	A	5.5	9.50	0	23,415
CI 40054	ZPcS	100	A	5.5	10.00	0	39,964
CI 40054	ZPcS	100	A	5.5	14.00	0	11,361
CI 40054	ZPcS	100	A	5.5	16.00	0	5360
CI 40060	CI 40054	75	B	5.0	8.00	-1	3050
CI 40060	CI 40054	75	B	5.0	9.00	-1	2480
CI 40060	CI 40054	75	B	5.0	7.00	-1	2921
CI 40060	CI 40054	75	B	5.0	6.00	-1	13,000
CI 40060	CI 40054	75	B	5.0	5.50	-1	29,465
CI 40060	CI 40054	75	B	5.0	5.25	-1	33,039
CI 40060	CI 40054	75	B	5.0	6.50	-1	8981
CI 40060	CI 40054	75	B	5.0	6.75	-1	5867
CI 40060	ZPcS	75	B	6.0	7.00	-1	2548
CI 40060	ZPcS	75	B	6.0	6.50	-1	3658
CI 40060	ZPcS	75	B	6.0	6.00	-1	3643
CI 40060	ZPcS	75	B	6.0	5.50	-1	18,279
CI 40060	ZPcS	75	B	6.0	5.00	-1	25,897
CI 40060	ZPcS	75	B	6.0	4.50	-1	44,481
CI 40060	ZPcS	75	B	6.0	4.00	-1	125,000

^a ZPcS = Zinc Phosphate coated Steel.

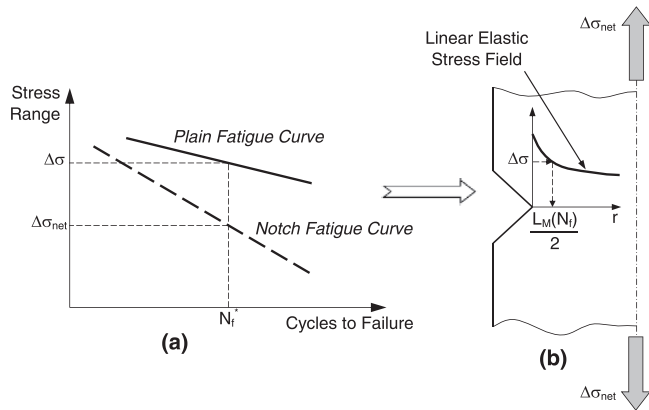


Fig. 8. Procedure to calibrate the material fatigue constants in the critical distance vs. number of cycles to failure relationship.

com) with the iron-carbon alloys used, the friction coefficient was set equal to 0.45 for the coated steel-to-CI 40054 contact and to 0.4 for the CI 40054-to-CI 40060 contact. These values for the friction coefficients are in agreement with the values reported by Mutoh and Tanaka [57] for different contact combinations involving both steel and cast iron.

The contact between the fretting pad and the specimen was defined using the target-contact algorithm that is available in Ansys® Workbench. In particular, the top surface of the specimen was defined as the target body while the circular surface of the pad defined as the contact body. In order to define the behaviour of the contact, the Augmented

Lagrange algorithm was included in the frictional contact region.

Having defined the three models, a mesh convergence study was carried out to determine the optimum mesh size to be used in the contact region. The loading sequence used for this purpose was based on three subsequent steps. Initially, the pad was moved downward to establish the contact with the specimen. Subsequently, a normal pressure was applied to the upper surface of the pad (Fig. 9c). Finally, a force was applied to the right-hand side of the specimen (Fig. 9c). The mesh convergence analysis was implemented by using from 5 up to 60 elements along the contact half-width, with a relatively coarser mesh being used away from the contact zone. A quadrilateral map mesh was employed to model both the pad and the specimen. At the end of any simulation, the normal stress components were extracted along the contact surface of the specimen and then used to assess the effect of the mesh density on the relevant stress distributions. Based on the results from this standard convergence analysis, the numerical stress analyses associated with the specimens being tested were performed by using along the contact half-width in between 20 and 40 elements, this corresponding to a mesh size ranging between 11 μm and 15 μm (Fig. 9d).

Finally, the accuracy and reliability of the optimised FE models was further checked by comparing the results from the numerical solutions with the corresponding results from the classic analytical solution due to Hertz. This was done in terms of contact half-width length and contact pressure distribution. The sound agreement between numerical and analytical solution further confirmed the validity of the FE models that were used to perform the necessary local linear-elastic stress analyses.

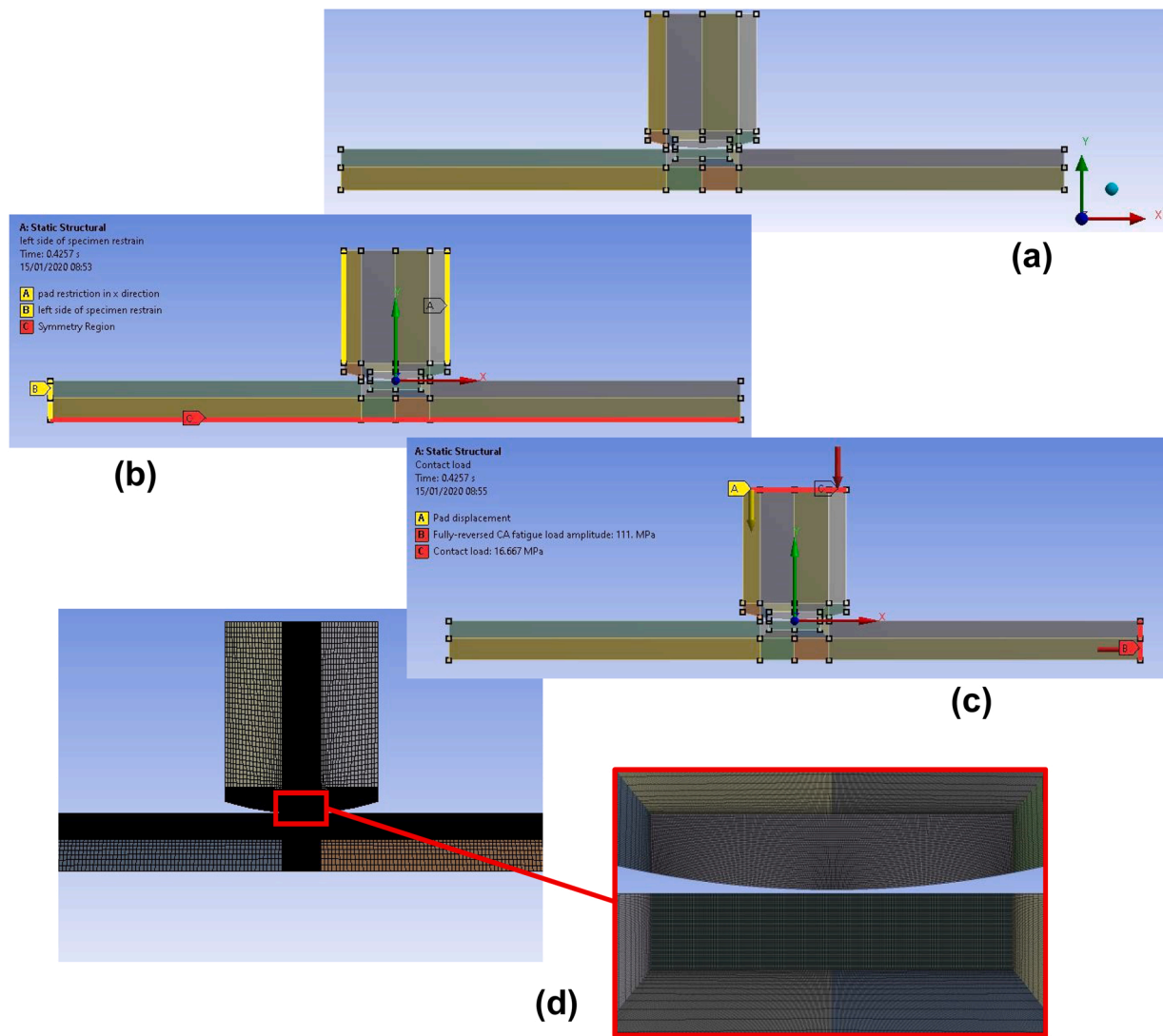


Fig. 9. Specimen with $R_p = 20$ mm pad: example of the numerical procedure followed to calculate the local linear-elastic stress fields in the contact region.

6.4. Accuracy

The FE models produced as described in the previous sub-section were used to post-process the experimental results summarised in Tables 2 and 4. In particular, these FE models were employed to determine the sub-surface distribution of the linear-elastic stress in the contact region of the specimens made of CI 40054 as well as of CI 40060. According to Figs. 3a and 3b, the focus paths were taken coincident with a straight line emanating from the leading edge of the contact zone and perpendicular to the contact surface itself.

The MWCM method's governing equations were calibrated as described in Section 6.1, with the L_M vs. N_f relationships being defined according to Eqs. (25) and (26).

The results generated under CA fretting fatigue loading and summarised in Table 2 were post-processed according to the approach described in Figs. 3 and 4. In contrast, the tests run under VA fretting fatigue loading that are summarised in Table 3 were post-process following the procedure described in Figs. 3 and 5. It is important to point out here that, as recommended by Palmgren [30] and Miner [31], the estimates under VA fretting fatigue loading were obtained by simply setting the critical value of the damage sum equal to unity.

The overall accuracy that was obtained by using the proposed methodology to predict the results summarised in Tables 2 and 4 is summarised in the experimental, N_f , vs. estimated, $N_{f,e}$, number of cycles

to failure diagram reported in Fig. 10. It can be seen from this error chart that the estimates all fall within an error factor of 2, with this holding true independently of material, pad radius and complexity of the applied fretting fatigue load history. This supports the idea that the methodology summarised in Figs. 3 to 5 is a powerful tool suitable for designing real mechanical assemblies against CA and VA fretting fatigue loading.

7. Conclusions

The present paper deals with the accuracy and reliability in estimating fretting fatigue lifetime of the MWCM applied along with the τ -MVM and the PM. The validation exercise being carried out was based on a large set of experimental results that were generated at the University of Sheffield, UK, under both CA and VA fretting fatigue loading. The specimens used in this campaign of experiments were made of two grey cast irons, i.e. CI 40054 and CI 40060.

The material properties that were needed to apply the proposed fretting fatigue lifetime estimation technique were determined experimentally by running conventional uniaxial and torsional fatigue tests.

The generated experimental results were post-processed by determining the relevant linear-elastic stress fields in the contact regions by using commercial FE software Ansys® Workbench.

Based on this validation exercise, the most relevant conclusions are summarised in the following bullet points.

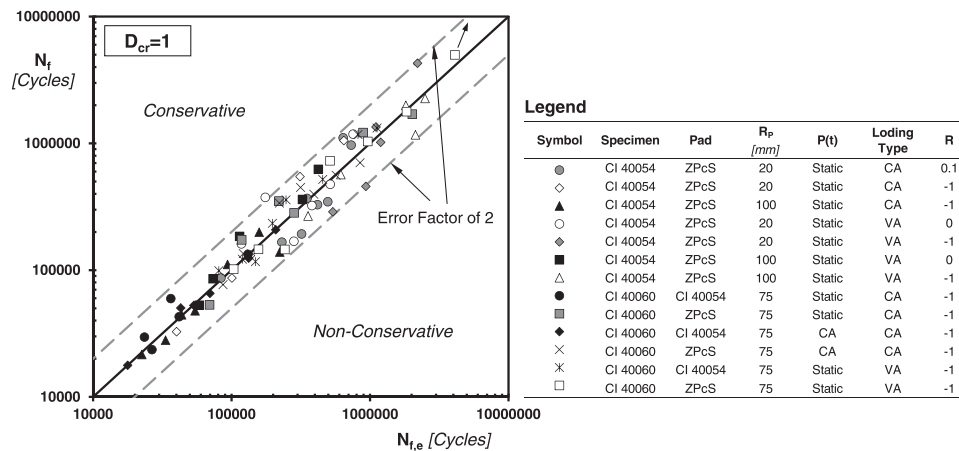


Fig. 10. Overall accuracy of the proposed CA/VA fretting fatigue life estimation technique (ZPcS = Zinc Phosphate coated Steel).

- Owing to its specific features, the approach formulated and validated in the present paper can be used to design real mechanical assemblies against CA/VA fretting fatigue loading by directly post-processing the relevant stress fields determined through conventional linear-elastic FE analyses.
- The use of the MWCM applied in conjunction with the τ -MVM and the PM returned estimates falling within an error factor of ± 2 .
- A very high level of accuracy can be reached provided that the proposed fretting fatigue design technique is calibrated by running appropriate experiments.
- As postulated by the classic theory due to Palmgren [30] and Miner [31], the lifetime under VA fretting fatigue loading of the tested iron-carbon alloys was estimated by setting the critical value of the damage sum invariably equal to unity.
- As far as VA fretting fatigue is concerned, more work needs to be done to devise a sound methodology allowing the critical value of the damage sum to be quantified in a rigorous, standardised way.

Declaration of Competing Interest

The authors declare that they have no known competing financial interests or personal relationships that could have appeared to influence the work reported in this paper.

Data Availability

All the data being used are available in the submitted paper.

Acknowledgements

Financial support for this Industrial CASE project from EPSRC (www.epsrc.ac.uk) and Cummins Inc. (www.cummins.com) is gratefully acknowledged.

References

- [1] Hills D, Nowell D. *Mechanics of Fretting Fatigue*. Dordrecht, The Netherlands: Kluwer Academic; 1994.
- [2] Johnson KL. Surface interaction between elastically loaded bodies under tangential forces. *Proc R Soc A* 1955;230:531–48.
- [3] Hills DA, Mugadu A. An overview of progress in the study of fretting fatigue. *J Strain Anal Eng Des* 2002;37(6):591–601.
- [4] Bhatti NA, Wahab MA. Fretting fatigue crack nucleation: a review. *Tribol Int* 2018; 121:121–38.
- [5] Giannakopoulos AE, Lindley TC, Suresh S, Chenut C. Similarities of stress concentration in contact at round punches and fatigue at notches: implication to fretting fatigue crack initiation. *Fatigue Fract Engng Mat Struct* 2000;23:561–71.
- [6] Nowell D, Dini D, Dyson I. The use of notch and short crack approaches to fretting fatigue threshold prediction: Theory and experimental validation. *Tribol Int* 2006; 39:1158–65.
- [7] Taylor D. *The Theory of Critical Distances: a new perspective in Fracture Mechanics*. Oxford, UK: Elsevier; 2007.
- [8] Susmel L. *The theory of critical distances: a review of its applications in fatigue*. *Eng Fract Mech* 2008;75(7):1706–24.
- [10] Bellett D, Taylor D, Marco S, Mazzeo E, Guillois J, Pircher T. The fatigue behaviour of three-dimensional stress concentrations. *Int J Fatigue* 2005;27(3): 207–21.
- [11] Peterson RE. Notch sensitivity. In: Sines G, Waisman JL, editors. *Metal Fatigue*. New York, USA: McGraw Hill; 1959. p. 293–306.
- [12] Ruiz C, Chen KC. Life assessment of dovetail joints between blades and discs in aero-engines. *Mech Eng Publ* 1986;1:187–94.
- [13] Fouvry S, Kapsa Ph, Sidoroff F, Vincent L. Identification of the characteristic length scale for fatigue cracking in fretting contacts. *J Phys IV* 1988;8(8). Pr8-159-166.
- [14] Fouvry S, Kapsa Ph, Vincent L. Fretting-Wear and Fretting-Fatigue: Relation through Mapping Concept. In: Höppener DW, Chandrasekaran V, Elliott CB, editors. *Fretting Fatigue: Current Technology and Practices*. West Conshohocken, PA: ASTM STP 1367, American Society of Testing and Materials; 2000. p. 49–64.
- [15] Araújo JA, Susmel L, Taylor D, Ferro JCT, Mamiya EN. On the use of the Theory of Critical Distances and the Modified Wöhler Curve Method to estimate fretting fatigue strength of cylindrical contacts. *Int J Fatigue* 2007;29:95–107.
- [16] Araújo JA, Susmel L, Pires MST, Castro FC. A multiaxial stress-based critical distance methodology to estimate fretting fatigue life. *Tribol Int* 2017;108:2–6.
- [17] Araújo JA, Castro FC, Matos IM, Cardoso RA. Life prediction in multiaxial high cycle fretting fatigue. *Int J Fatigue* 2020;134:105504.
- [18] Gailliege T, Doca T, Araújo JA, Ferreira JLA. Fretting life of the Al7050-T7451 under out-of-phase loads: Numerical and experimental analysis. *Theor Appl Fract Mech* 2020;106:102492.
- [19] Gandiolle C, Garcin S, Fouvry S. A non-collinear fretting-fatigue experiment to compare multiaxial fatigue criteria: critical shear plane strategy is better than invariant formulations. *Tribol Int* 2017;108:57–68.
- [20] Kantimathi A, Alic J. The effects of periodic high loads on fretting fatigue. *J Eng Mater Technol* 1981;103(3):223–8.
- [21] Mutoh Y, Tanaka K, Kondoh M. Fretting fatigue in jis s45c steel under two-step block loading: solid-mechanics, strength of materials. *JSM Int J* 1987;30(261): 386–93.
- [22] Mutoh Y, Tanaka K, Kondoh M. Fretting fatigue in sup9 spring steel under random loading. *JSM Int J Ser 1 Solid Mech. Strength Mater* 1989;32(2):274–81.
- [23] Troshchenko V, Dragan V, Semenjuk S. Fatigue damage accumulation in aluminium and titanium alloys subjected to block program loading under conditions of stress concentration and fretting. *Int J Fatigue* 1999;21(3):271–9.
- [24] Cortez R, Mall S, Calcaterra JR. Investigation of variable amplitude loading on fretting fatigue behavior of ti-6al-4v. *Int J Fatigue* 1999;21(7):709–17.
- [25] Kinyon SE, Hoepfner DW. Spectrum load effects on the fretting behavior of Ti-6Al-4V. ASTM STP 1367. In: Höppener DW, Chandrasekaran V, Elliott CB, editors. *Fretting Fatigue: Current Technology and Practices*. West Conshohocken, PA: American Society of Testing and Materials; 2000. p. 100–18. ASTM STP 1367.
- [26] Kondo Y, Sakae C, Kubota M, Kitahara H, Yanagihara K. Fretting fatigue under variable loading below fretting fatigue limit. *Fatig Fract Eng Mater Struct* 2006;29 (3):191–9.
- [27] Massingham M, Irving P. The effect of variable amplitude loading on stress distribution within a cylindrical contact subjected to fretting fatigue. *Tribol Int* 2006;39(10):1084–91.
- [28] Gandiolle C, Fouvry S. Fretting fatigue crack propagation rate under variable loading conditions. *Frat Ed Integrita Strutt* 2016;10(35):232–41.
- [29] Pinto AL, Cardoso RA, Talemi R, Araujo JA. Fretting fatigue under variable amplitude loading considering partial and gross slip regimes: numerical analysis. *Tribol Int* 2020;146(93):106–99.
- [30] A. Palmgren Die Lebensdauer von Kugellagern. *Verfahrenstechnik Berlin*, 68, 1924, pp. 339–341.
- [31] Miner MA. Cumulative damage in fatigue. *J Appl Mech* 1945;67:AI59–64.

- [32] Susmel L, Lazzarin P. A Bi-parametric Modified Wöhler Curve for high cycle multiaxial fatigue assessment. *Fatigue Fract Eng Mater Struct* 2002;25:63–78.
- [33] Lazzarin P, Susmel L. A stress-based method method to predict lifetime under multiaxial fatigue loadings. *Fatigue Fract Eng Mater Struct* 2003;26:1171–87.
- [34] Susmel L. A simple and efficient numerical algorithm to determine the orientation of the critical plane in multiaxial fatigue problems. *Int J Fatigue* 2010;32:1875–83.
- [35] Susmel L, Tovo R, Socie DF. Estimating the orientation of Stage I crack paths through the direction of maximum variance of the resolved shear stress. *Int J Fatigue* 2014;58:94–101.
- [36] Susmel L, Tovo R, Benasciutti D. A novel engineering method based on the critical plane concept to estimate lifetime of weldments subjected to variable amplitude multiaxial fatigue loading. *Fatigue Fract Eng Mater Struct* 2009;32:441–59.
- [37] Susmel L, Taylor D. A critical distance/plane method to estimate finite life of notched components under variable amplitude uniaxial/multiaxial fatigue loading. *Int J Fatigue* 2012;38:7–24.
- [38] Susmel L. Four stress analysis strategies to use the Modified Wöhler Curve Method to perform the fatigue assessment of weldments subjected to constant and variable amplitude multiaxial fatigue loading. *Int J Fatigue* 2014;67:38–54.
- [39] Susmel L. Multiaxial fatigue limits and material sensitivity to non-zero mean stresses normal to the critical planes. *Fatigue Fract Eng Mater Struct* 2008;31:295–309.
- [40] Susmel L. *Multiaxial Notch Fatigue: from nominal to local stress-strain quantities*. Cambridge, UK: Woodhead & CRC; 2009.
- [41] Susmel L, Tovo R, Lazzarin P. The mean stress effect on the high-cycle fatigue strength from a multiaxial fatigue point of view. *Int J Fatigue* 2005;27:928–43.
- [42] Kaufman RP, Topper T. The influence of static mean stresses applied normal to the maximum shear planes in multiaxial fatigue. In: Carpinteri A, de Freitas M, Spagnoli A, editors. *Biaxial and Multiaxial fatigue and Fracture*. Elsevier and ESIS; 2003. p. 123–43.
- [43] Kouanga CT, Jones JD, Revill I, Wormald A, Nowell D, Dwyer-Joyce RS, et al. On the estimation of finite lifetime under fretting fatigue loading. *Int J Fatigue* 2018;112:138–52.
- [44] Susmel L, Taylor D. A novel formulation of the theory of critical distances to estimate lifetime of notched components in the medium-cycle fatigue regime. *Fatigue Fract Eng Mater Struct* 2007;30:567–81.
- [45] Susmel L, Taylor D. The Modified Wöhler curve method applied along with the theory of critical distances to estimate finite life of notched components subjected to complex multiaxial loading paths. *Fatigue Fract Eng Mater Struct* 2008;31:1047–64.
- [46] Neuber H. *Theory of Notch Stresses: Principles for Exact Calculation of Strength with Reference to Structural Form and Material*. II ed. Berlin: Springer Verlag; 1958.
- [47] Susmel L. A unifying approach to estimate the high-cycle fatigue strength of notched components subjected to both uniaxial and multiaxial cyclic loadings. *Fatigue Fract Eng Mater Struct* 2004;27:391–411.
- [48] Bellett D, Taylor D, Marco S, Mazzeo E, Guillois J, Pircher T. The fatigue behaviour of three-dimensional stress concentrations. *Int J Fatigue* 2005;27:207–21.
- [49] Haibach E. *Betriebsfestigkeit—Verfahren und Daten zur Bauteilberechnung*. Düsseldorf, Germany: VDI-Verlag GmbH; 1989.
- [50] Sonsino CM. Course of SN-curves especially in the high-cycle fatigue regime with regard to component design and safety. *Int J Fatigue* 2007;29:2246–58.
- [51] Matsuishi M, Endo T. *Fatigue of Metals Subjected to Varying Stress*. Fukuoka, Japan: Presented to the Japan Society of Mechanical Engineers; 1968.
- [52] Downing SD, Socie DF. Simple rainflow counting algorithms. *Int J Fatigue* 1982;4(1):31–40.
- [53] Sonsino CM. Fatigue testing under variable amplitude loading. *Int J Fatigue* 2007;29(6):1080–9.
- [54] Al Zamzami I, Susmel L. On the accuracy of nominal, structural, and local stress based approaches in designing aluminium welded joints against fatigue. *Int J Fatigue* 2017;101(2):137–58.
- [55] Susmel L. Notches, nominal stresses, fatigue strength reduction factors and constant/variable amplitude multiaxial fatigue loading. *Int J Fatigue* 2022;162:106941.
- [56] Susmel L, Taylor D. The theory of critical distances to estimate lifetime of notched components subjected to variable amplitude uniaxial fatigue loading. *Int J Fatigue* 2011;33:900–11.
- [57] Mutoh Y, Tanaka K. Fretting fatigue in several steel and cast iron. *Wear* 1988;125:175–91.